Direct measurements of anisotropic energy transfers in a rotating turbulence experiment

Cyril Lamriben, Pierre-Philippe Cortet, and Frédéric Moisy
Laboratoire FAST, CNRS, Univ Paris-Sud, UPMC Univ Paris 06, Bât. 502, Campus universitaire, 91405 Orsay, France

We investigate experimentally the influence of a background rotation on the energy transfers in decaying grid turbulence. The anisotropic energy flux density, $\mathbf{F}(\mathbf{r}) = \langle \delta\mathbf{u}\,(\delta\mathbf{u})^2 \rangle$, where $\delta\mathbf{u}$ is the vector velocity increment over separation $\mathbf{r}$, is determined for the first time using Particle Image Velocimetry. We show that rotation induces an anisotropy of the energy flux $\nabla \cdot \mathbf{F}$, which leads to an anisotropy growth of the energy distribution $E(\mathbf{r}) = \langle (\delta\mathbf{u})^2 \rangle$, in agreement with the Kármán-Howarth-Monin equation. Surprisingly, our results prove that this anisotropy growth is essentially driven by a nearly radial, but orientation-dependent, energy flux density $\mathbf{F}(\mathbf{r})$.

The energy cascade from large to small scales, and the associated Kolmogorov 4/5th law, are recognized as the most fundamental results of homogeneous and isotropic turbulence [1, 2]. In the presence of a background rotation, a situation which is relevant for most geophysical and astrophysical flows, the scale-to-scale energy transfers are modified by the Coriolis force, yielding a gradual columnar structuring of turbulence along the rotation axis [3–7]. The Taylor-Proudman theorem is often invoked, however improperly, to justify the resulting quasi-2D nature of turbulence under rotation. Indeed, this theorem is a purely linear result, which applies only in the limit of zero Rossby number (i.e. infinite rotation rate), and is therefore incompatible with turbulence; it cannot describe the anisotropic energy transfers responsible for the non-trivial organization of rotating turbulence which are a subtle non-linear effect taking place only at non-zero Rossby number. To date, no direct evidence for these anisotropic energy transfers towards the 2D state in the physical space has been obtained. In this Letter, we report for the first time direct measurements of the physical-space energy transfers in decaying rotating turbulence using Particle Image Velocimetry (PIV), and provide new insight into the anisotropy growth of turbulence at finite, and hence geophysically relevant, Rossby number.

If homogeneity (but not necessarily isotropy) holds, the energy distribution and energy flux density in the space of separations $\mathbf{r}$ are described by the fields

$$E(\mathbf{r},t) = \langle (\delta\mathbf{u})^2 \rangle \qquad \text{and} \qquad \mathbf{F}(\mathbf{r},t) = \langle \delta\mathbf{u}\,(\delta\mathbf{u})^2 \rangle, \quad (1)$$

where $\mathbf{u}(\mathbf{x},t)$ is the turbulent velocity, $\delta\mathbf{u} = \mathbf{u}(\mathbf{x}+\mathbf{r},t) - \mathbf{u}(\mathbf{x},t)$ is the velocity vector increment over $\mathbf{r}$ (Fig. 1), and $\langle\cdot\rangle$ denotes spatial and ensemble averages. These key quantities satisfy the Kármán-Howarth-Monin (KHM) equation [1, 8], which describes the evolution of the energy distribution in the space of separations,

$$\frac{1}{2}\frac{\partial}{\partial t} R = \frac{1}{4}\nabla \cdot \mathbf{F} + \nu \nabla^2 R, \quad (2)$$

where $R(\mathbf{r},t) = \langle \mathbf{u}(\mathbf{x},t) \cdot \mathbf{u}(\mathbf{x}+\mathbf{r},t) \rangle = \langle \mathbf{u}^2 \rangle - E(\mathbf{r},t)/2$ is the two-point velocity correlation and ν the kinematic viscosity. Importantly, this equation is still valid for homogeneous anisotropic turbulence [9], and in particular for axisymmetric turbulence in a rotating frame (here axisymmetry is to be understood in the statistical sense, with respect to $\mathbf{r}$). For stationary (forced) turbulence, this equation reduces to $\nabla \cdot \mathbf{F} = -4\,\epsilon$ in the inertial range, where ϵ stands for the rates of injected and dissipated energy. In the isotropic case, this constant-flux relation yields a purely radial flux density, $\mathbf{F}(\mathbf{r}) = -(4/3)\,\epsilon\,\mathbf{r}$, describing the usual energy cascade from large to small scales. This result is actually identical to the celebrated Kolmogorov's 4/5th law, classically expressed in terms of the 3rd order longitudinal structure function, $\langle \delta u_L^3 \rangle = -(4/5)\,\epsilon\,r$, where $\delta u_L = \delta\mathbf{u} \cdot \mathbf{r}/r$ is the longitudinal velocity increment.

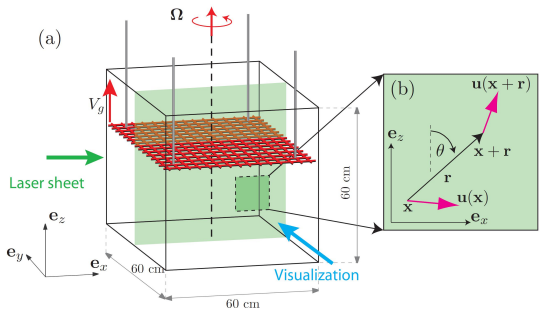

FIG. 1: (a) Experimental setup. The water-filled tank is rotating at $0 \le \Omega \le 1.68$ rad s^{-1}. The grid is towed from the bottom to the top, and PIV measurements are performed in the vertical plane (x, z) in the rotating frame during the turbulence decay. (b) Definition of the vector velocity increment $\delta\mathbf{u} = \mathbf{u}(\mathbf{x}+\mathbf{r}) - \mathbf{u}(\mathbf{x})$.

In decaying rotating homogeneous turbulence, Eq. (2) shows that, starting from an isotropic initial energy distribution $E(\mathbf{r},0)$, an anisotropy growth in $E(\mathbf{r},t)$ is expected if an anisotropic energy flux $\nabla\cdot\mathbf{F}$ is induced by the Coriolis force. However, the flux density $\mathbf{F}(\mathbf{r})$ itself has never been measured, and its precise form, which reveals the fundamental action of rotation on turbulence, is so far unknown. The only experimental attempts to characterize the energy transfers in rotating turbulence were restricted to measurements of $\langle \delta u_L^3 \rangle$ in the plane normal to

the rotation axis [10, 11], hence ignoring the anisotropic nature of those transfers. Recent theoretical efforts have been made to generalize the 4/5th law, assuming weak anisotropy [12], or considering the full anisotropic problem but restricted to the stationary case [9].

Experiments.- The experimental setup is similar to the one described in Ref. [13], and is briefly recalled here (Fig. 1a). Turbulence is generated by towing a square grid at a velocity $V_g = 1.0$ m s^{-1} from the bottom to the top of a cubic glass tank, of side 60 cm, filled with 52 cm of water. The grid consists in 8 mm thick bars with a mesh size $M = 40$ mm. The whole setup is mounted on a precision rotating turntable of 2 m in diameter. Runs for three rotation rates, $\Omega = 0.42, 0.84$ and 1.68 rad s^{-1} (4, 8 and 16 rpm), as well as a reference run without rotation, have been carried out. The initial Reynolds number based on the grid mesh is $Re_g = V_g M/\nu = 40\,000$, and the initial Rossby number $Ro_g = V_g/2\Omega M$ ranges from 7.4 to 30, indicating that the flow in the close wake of the grid is fully turbulent and weakly affected by rotation. During the turbulence decay, the instantaneous Rossby number, $Ro(t) = \langle \mathbf{u}^2 \rangle^{1/2}/2\Omega M$, decreases with time down to 10^{-2}, spanning a range in which influence of rotation is expected. An important concern about grid turbulence experiments in a confined rotating domain is the excitation of reproducible inertial modes [14]. Here, we use the modified grid introduced in Ref. [13], which was shown to significantly reduce the generation of these modes. Consequently, turbulence can be considered here as almost freely decaying and homogeneous, a necessary condition for the validity of the KHM equation (2).

Velocity measurements are performed in the rotating frame using a corotating PIV system. Two velocity components (u_x, u_z) are measured, in a vertical 16×16 cm^2 field of view, where z is the rotation axis. During the decay of turbulence, 60 image pairs are acquired by a double-frame 2048^2 pixels camera, at a rate of 1 pair per second. The PIV resolution, 1.3 mm, is sufficient to resolve the inertial range but fails to resolve the dissipative scale (the Kolmogorov scale is of the order of 0.2 mm right after the grid translation [11]).

Only surrogates of $E(\mathbf{r})$ and $\mathbf{F}(\mathbf{r})$ (1) can be computed from the measured 2D velocity fields. These surrogate quantities are defined as

$$\widetilde{E}(\mathbf{r}) = \langle \delta u_x^2 + \delta u_z^2 \rangle_{x,z}, \quad \widetilde{\mathbf{F}}(\mathbf{r}) = \langle \delta \mathbf{u} (\delta u_x^2 + \delta u_z^2) \rangle_{x,z}, \quad (3)$$

where the spatial average is restricted to the measurement plane, and $\mathbf{r} = r_x \mathbf{e}_x + r_z \mathbf{e}_z$. For each time after the grid translation, these quantities are computed for all separations $\mathbf{r}$ in the PIV field of view, and are ensemble-averaged over 600 realizations of the turbulence decay. The fields $\widetilde{E}(\mathbf{r})$ and $\widetilde{\mathbf{F}}(\mathbf{r})$ are remapped on a spherical coordinate system (r, θ, ϕ), where $r = |\mathbf{r}|$, and θ is the polar angle between $\mathbf{e}_z$ and $\mathbf{r}$; the invariance with respect to the (non-measured) azimuthal angle ϕ is assumed by axisymmetry. Although relations between the surrogates (3) and the exact 3-components quantities (1) can be derived for isotropic turbulence, no general relation holds in the anisotropic case, so we do not apply any correction weight in $\widetilde{E}$ and $\widetilde{\mathbf{F}}$. Since only the surrogates are considered in this paper, we simply drop the tildes $\widetilde{\cdot}$ in the following.

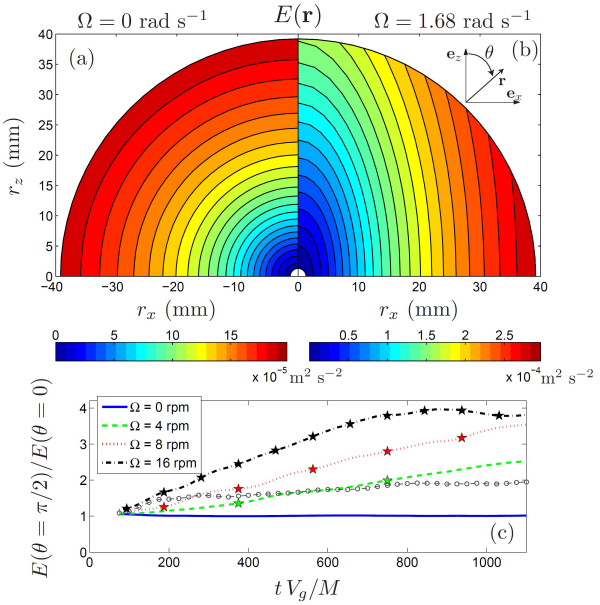

FIG. 2: Energy distribution $E(\mathbf{r})$ at time $t\,V_g/M = 400$ after the grid translation, for (a) $\Omega = 0$, and (b) $\Omega = 1.68$ rad s^{-1} (16 rpm). (c) Horizontal-to-vertical energy ratio as a function of time at scale $r = 10$ mm for various Ω; $\circ$: additional curve at $r = 30$ mm for $\Omega = 16$ rpm. Stars indicate integer numbers of tank rotations.

The convergence of the statistics from experimental measurements is very delicate to achieve, in particular for the computation of $\mathbf{F}(\mathbf{r})$, which is a 3rd order moment of a zero-mean velocity increment. We found that, using a set of 600 realizations of the turbulence decay, a convergence better than 5% at small scales, and of the order of 20% at scales $r \simeq M$, could be achieved for $\mathbf{F}(\mathbf{r})$. The convergence for $E(\mathbf{r})$ is better than 1% for all scales up to $r \simeq M$.

Energy distribution.- The map of energy distribution $E(\mathbf{r})$ for separations $\mathbf{r}$ in the vertical plane is plotted in Fig. 2, at a time $t\,V_g/M = 400$ after the grid translation. The iso-E curves are found nearly circular for $\Omega = 0$ (Fig. 2a), showing the good level of isotropy of our grid turbulence without rotation. On the other hand, they are highly anisotropic at the same time for $\Omega = 16$ rpm (corresponding to 4.3 tank rotations), with a strong depletion of $E(\mathbf{r})$ along the rotation axis z (Fig. 2b). The depletion of $E(\mathbf{r})$ corresponds to an enhanced velocity correlation $R(\mathbf{r})$ along the rotation axis, reflecting the classical trend towards a 2D flow invariant along z. Importantly, an isotropic energy distribution is found in the 3 rotating cases just after the grid translation, as demonstrated in Fig. 2(c) where the time evolution of the horizontal-

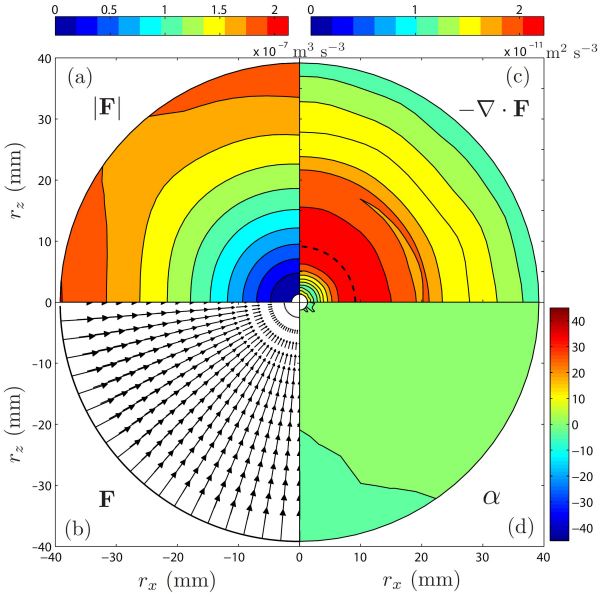

FIG. 3: Energy flux density $\mathbf{F}(\mathbf{r})$ in the non-rotating case, at time $t\,V_g/M = 400$ after the grid translation. (a) Flux density magnitude $|\mathbf{F}|$. (b) Raw vector field $\mathbf{F}$. (c) Energy flux $\nabla \cdot \mathbf{F}$. (d) Deviation angle $\alpha(\mathbf{r})$, defined as $\sin\alpha(\mathbf{r}) = \mathbf{e}_y \cdot (\mathbf{e}_r \times \mathbf{F})/|\mathbf{F}|$; iso-angle lines are separated by 5°. The dashed line in (c) shows the "crest line", following the local maximum of $-\nabla \cdot \mathbf{F}$.

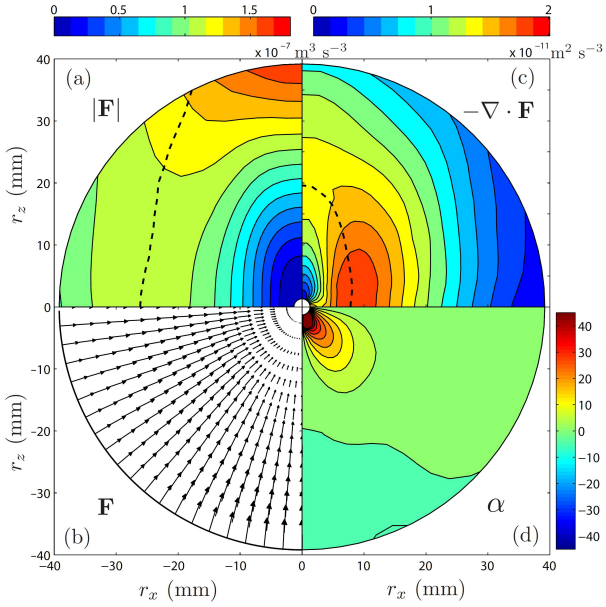

FIG. 4: Energy flux density $\mathbf{F}(\mathbf{r})$ in the rotating case (Ω = 16 rpm), at time $t\,V_g/M = 400$ after the grid translation. Same layout as for Fig. 3.

to-vertical energy ratio $E(\theta = 0)/E(\theta = \pi/2)$ is plotted for an inertial-range separation $r = 10$ mm. This confirms that the initial grid turbulence is isotropic even when $\Omega \neq 0$, and that the subsequent anisotropy growth is a pure effect of the background rotation. Fig. 2(c) also shows that the anisotropy growth rate is essentially proportional to Ω [5, 7]. Interestingly, the anisotropy is found more pronounced at small scales, as shown by the lower anisotropy ratio plotted for $r = 30$ mm. It is worth noting that this stronger anisotropy at small scales is in contradiction with the naive assumption that large scales, having a slower dynamics, are more affected by rotation than the faster and supposedly still 3D small scales.

Energy transfers: isotropic case.- We now turn to the energy flux density, and we first present in Fig. 3(b) measurements of $\mathbf{F}(\mathbf{r})$ for $\Omega = 0$, at the same time $tV_g/M = 400$. This vector field is found remarkably radial, pointing towards the origin, giving direct evidence of the isotropic energy cascade in the physical space, from the large to the small scales, in the non-rotating case. Finer assessment of the isotropy of $\mathbf{F}$ can be achieved by introducing the following three scalar quantities: the deviation angle $\alpha(\mathbf{r})$ from the radial direction (Fig. 3d), the magnitude $|\mathbf{F}|$ (Fig. 3a), and the energy flux $\nabla \cdot \mathbf{F}$ (Fig. 3c). The very weak angle measured for $r \leq M$, $\alpha(\mathbf{r}) \simeq 2^o \pm 2^o$, confirms the almost purely radial nature of $\mathbf{F}$. The isotropy of the flux density magnitude is not as good: the iso-$|\mathbf{F}|$ are nearly circular up to $r \simeq 30$ mm, but shows slight departure from isotropy at larger r, suggesting that this quantity is very sensitive to a residual anisotropy of the large-scale flow. However, the iso-$\nabla \cdot \mathbf{F}$ remain remarkably circular up to $r \simeq M$, showing that the residual large-scale anisotropy has indeed a weak influence on the energy flux for $r \leq M$. The energy flux $\nabla \cdot \mathbf{F}$ shows a broad negative minimum in an annular region spanning over $r \simeq 5 - 20$ mm, providing an indication of the extent of the inertial range (we recall that, in the inertial range, $\nabla \cdot \mathbf{F} = -4\epsilon$), and decreases to zero both at small and large scales.

Energy transfers: rotating case.- We consider now the energy transfers in the rotating case, shown in Fig. 4 at the same time $t\,V_g/M = 400$. Interestingly, the flux density $\mathbf{F}$ is found to remain nearly radial for all separations, in qualitative agreement with recent predictions [9], except at the smallest scales, for $r < 10$ mm, where a marked deflection towards the rotation axis is observed. Such horizontally tilted $\mathbf{F}$ is indeed consistent with an asymptotic 2D flow, for which $\mathbf{F}$ must be a strictly horizontal vector, function of the horizontal component of the separation only. This small-scale anisotropy is best appreciated from the map of the deviation angle α (Fig. 4d), showing a region of nonzero α at small scale only. Note that horizontally tilted $\mathbf{F}$ exists only for intermediate angle θ since axisymmetry requires a radial $\mathbf{F}$ for $\theta = 0$ and $\pi/2$. The 2D trend is remarkably weak in terms of the orientation of $\mathbf{F}(\mathbf{r})$ in the inertial range, compared to the strong anisotropy observed for the energy distribution $E(\mathbf{r})$ at comparable scales: α is only in the range $0 - 10^o$ in the inertial range, and increases up to $25^o \pm 5^o$ for $r \to 0$, with no significant dependence with Ω.

If we focus on the flux density magnitude $|\mathbf{F}|$, which is essentially given by the radial component $-F_r = -\mathbf{F} \cdot \mathbf{e}_r$, a clear anisotropy is now found at all scales. This

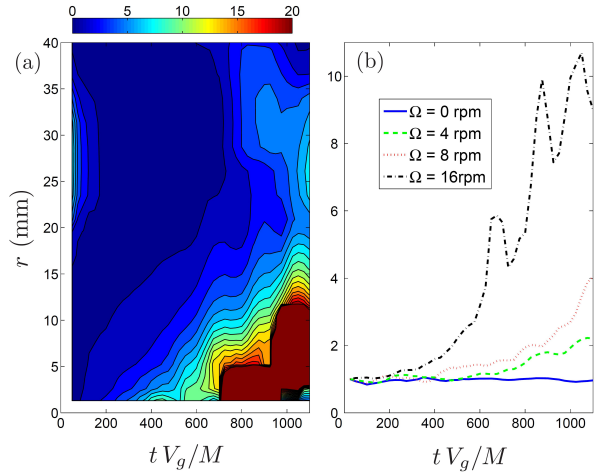

FIG. 5: (a) Spatio-temporal diagram of the horizontal-to-vertical energy flux ratio, $\nabla\cdot\mathbf{F}(\theta=\pi/2)/\nabla\cdot\mathbf{F}(\theta=0)$, showing the anisotropy growing from small to large scales. (b) Time evolution of the energy flux ratio at scale $r = 10$ mm for various Ω.

suggests that the anisotropy of the energy transfers is mostly driven by the θ-dependence of F_r, and not by the growth of a nonzero polar component $F_\theta = \mathbf{F}\cdot\mathbf{e}_\theta$. The maximum of $|\mathbf{F}|$ is systematically encountered near the rotation axis, at rather large scales, centered around 50-80 mm (outside the range shown in Fig. 4a). The local maximum of $|\mathbf{F}|$ on the horizontal axis is encountered at smaller scales, as evidenced by the crest line in Fig. 4(a).

The flux map $\nabla\cdot\mathbf{F}$ (Fig. 4c) shows an overall anisotropic structure similar to that of $|\mathbf{F}|$, but essentially shifted towards smaller scales. The inertial range, where the flux $\nabla\cdot\mathbf{F}$ is negative and approximately constant, becomes vertically elongated as time proceeds. Actually, although $|\mathbf{F}|$ is maximum along the rotation axis, it is spread over a wider range of scales, leading to a weaker flux $\nabla\cdot\mathbf{F}$ along z than along x, and hence a less intense vertical energy cascade. Here again, this is consistent with a 2D trend, which should yield a vanishing energy flux along the rotation axis. The horizontal-to-vertical flux ratio in Fig. 5 illustrates this vanishing vertical energy cascade as time proceeds, an effect which is clearly enhanced as the rotation rate is increased.

It must be noted that the spatial structure of the flux $\nabla\cdot\mathbf{F}$ is in good qualitative agreement with the KHM equation (2). Indeed, neglecting the viscous term, the vertically elongated region where $\nabla\cdot\mathbf{F} < 0$ induces a stronger reduction of the velocity correlation R along x than along z, resulting in a relative growth of the vertical correlation along z, and hence a vertical depletion of the energy distribution $E = 2(\langle\mathbf{u}^2\rangle - R)$. We can conclude that the measured flux density $\mathbf{F}$ contains, through its divergence, a spatial structure consistent with the anisotropy growth of E observed in Fig 2. Interestingly, in line with the stronger anisotropy of $E(\mathbf{r})$ found at smaller scales, the flux is also found more anisotropic at smaller scales. This is clearly demonstrated by the spatio-temporal diagram in Fig. 5(a), showing that the anisotropy first appears at small scales, and then propagates towards larger scales as time proceeds.

Conclusion.- We report the first direct measurements of the energy flux density $\mathbf{F}$ in the physical space in a decaying rotating turbulence experiment. Although the alternative description of the energy transfers in the spectral space is more natural for theory or numerics [2–4, 6], the direct use of the KHM equation (2) in the physical space, which is better suited for experiments, reveals here new and unexpected behaviors. The spatial structure of the measured energy distribution and energy flux $\nabla\cdot\mathbf{F}$ are found in good qualitative agreement with the KHM equation which, to our knowledge, has never been assessed experimentally. Surprisingly, the anisotropy growth of the energy distribution is primarily driven by an almost radial, but orientation-dependent, flux density $\mathbf{F}$, except at small scales where $\mathbf{F}$ shows a horizontal tilt, compatible with a trend towards a 2D state. It is also demonstrated that the anisotropy is paradoxically stronger at small scales, and propagates towards larger scales as time proceeds, an unexpected result which should motivate new theoretical efforts.

We acknowledge S. Galtier, J.-P. Hulin, and M. Rabaud for fruitful discussions, and Triangle de la Physique for funding of the "Gyroflow" platform.

[1] U. Frisch, *Turbulence - The Legacy of A. N. Kolmogorov* (Cambridge University Press, Cambridge, 1995).
[2] P. Sagaut and C. Cambon, *Homogeneous Turbulence Dynamics* (Cambridge University Press, Cambridge, 2008).
[3] C. Cambon and L. Jacquin, J. Fluid Mech. **202**, 295 (1989).
[4] F. Waleffe, Phys. Fluids A **5**, 677 (1993).
[5] P.J. Staplehurst, P.A. Davidson, and S.B. Dalziel, J. Fluid Mech. **598**, 81 (2008).
[6] P.D. Mininni and A. Pouquet, Phys. Fluids **22**, 035106 (2010).
[7] F. Moisy *et al.*, J. Fluid Mech. **666**, 5 (2011).
[8] A. S. Monin and A. M. Yaglom, *Statistical Fluid Mechanics*, vol. 2 (MIT Press, Cambridge, 1975).
[9] S. Galtier, Phys. Rev. E **80**, 046301 (2009).
[10] C. N. Baroud *et al.*, Phys. Rev. Lett. **88**, 114501 (2002).
[11] C. Morize, F. Moisy, and M. Rabaud, Phys. Fluids **17**, 095105 (2005).
[12] S. Chakraborty and J. K. Bhattacharjee, Phys. Rev. E **76**, 036304 (2007).
[13] C. Lamriben *et al.*, Phys. Fluids **23**, 015102 (2011).
[14] G. P. Bewley *et al.*, Phys. Fluids **19**, 071701 (2007).